ELSEVIER

Surface Science 373 (1997) 129–144

surface science

The surface chemistry of methylene iodide adsorbed on clean and oxygen-covered Mo(100): formation and chemistry of carbenes

Gefei Wu, B.F. Bartlett, W.T. Tysoe *

Department of Chemistry and Laboratory for Surface Studies, University of Wisconsin–Milwaukee, Milwaukee, WI 53211, USA

Received 22 May 1996; accepted for publication 3 September 1996

Abstract

Carbene species are grafted onto Mo(100) by the thermal decomposition of methylene iodide, where the decomposition is followed using ultraviolet photoelectron spectroscopy. Carbenes hydrogenate to methane by reaction with surface hydrogen via a second-order reaction with an activation energy of 21 ± 2 kJ mol^{-1}. Experiments with deuterium show that there appears to be no hydrogen–deuterium exchange between the carbene and surface hydrogen. The carbene decomposition temperature increases with the addition of oxygen to the surface, and this effect is ascribed to the effect of site blocking rather than a chemical modification of the adsorbed carbene by coadsorbed oxygen. Similarly, although the methane desorption temperature increases with increasing oxygen coverage, this effect is found to be due to a change in the surface coverage of carbene and hydrogen rather than a chemical modification of the carbene itself. Finally, no ethylene or ethane are found to desorb from the surface.

Keywords: Chemisorption; Low index single crystal surfaces; Methylene iodide; Molybdenum; Soft X-ray photoelectron spectroscopy; Thermal desorption; Thermal desorption spectroscopy

1. Introduction

C_1 species constitute the chemical "building blocks" for a number of catalyzed hydrocarbon conversion reactions. For example, hydrocarbon synthesis using CO and hydrogen involves the initial formation of these species which can then polymerize on the surface to form hydrocarbons [1–13], a reaction also catalyzed by metallic molybdenum [14]. Olefin metathesis has been proposed to be initiated by carbene formation, which then reacts further with an alkene to form a metallacycle which decomposes to yield metathesis products [15–31]. This reaction may also proceed at high temperatures via carbene polymerization to form higher hydrocarbons [32,33]. It has also recently been shown that a bifunctional molybdenum oxide + zeolite catalyst can convert methane into benzene where the reaction proceeds via an initial molybdenum-oxide catalyzed formation of ethylene which is then converted into benzene by the zeolite [34–36]. It has been proposed, in the latter case, that the active form of the catalyst is a molybdenum carbide, but the nature of the molybdenum-based catalyst remains to be firmly established. Clearly, however, this reaction requires the participation of C_1 species in the formation of ethylene. It has also been shown that the activity of molybdenum-based metathesis catalysts depends strongly on the metal oxidation state [37,38], and recent studies on model oxide

* Corresponding author. Fax: 414 229 5530; e-mail: wtt@alpha2.csd.uwm.edu

0039-6028/97/$17.00
PII S0039-6028(96)01164-8

catalysts have suggested that MoO_2 provides the most active catalyst for this reaction [39]. It has also been found that oxygen overlayers on molybdenum affect the activity of the catalyst, although they do not provide catalysts which are as active as the oxide itself [33,39].

In order to investigate this chemistry, we have formed adsorbed CH_2 species by decomposing methylene iodide on the surface of either clean or oxygen-covered Mo(100). This is now a well-established general strategy for grafting hydrocarbon fragments onto surfaces, since the C–I bond is relatively weak and iodine is abstracted on adsorption to form an adsorbed hydrocarbon fragment and deposit atomic iodine [40–43]. This chemistry is tracked in this work using ultraviolet photoelectron spectroscopy, which has the additional advantage that it allows the electronic structure of the resulting species to be probed so that this can be correlated with changes in chemical reactivity as well as by using temperature-programmed desorption. It has previously been demonstrated that methylene iodide can react on Mo(110) to form adsorbed carbenes and that these can react with hydrogen to form methane [44]. Adsorbed methylene is shown to react similarly on Mo(100). The structure of oxygen on Mo(100) has also been extensively studied, where oxygen coverages can be calibrated by an array of LEED patterns exhibited by oxygen overlayers as a function of coverage [45–52].

2. Experimental

Two pieces of equipment were used for these experiments. The first has been described in detail elsewhere [53]. Briefly, it consists of an ion- and sublimation-pumped, bakeable, ultrahigh vacuum chamber operating at a base pressure of $<1\times10^{-10}$ Torr following bakeout. The Mo(100) sample is mounted to the end of a rotatable, carousel geometry manipulator by means of 0.5 mm-diameter tantalum wires spot-welded to 2 mm-diameter tantalum heating rods. In order to improve the thermal contact between the heating wires and to facilitate spot-welding of the sample, the Mo(100) single crystal is square, so that the thin tantalum wires are attached along the top and bottom edges of the sample. This, in principle, allows the sample to be resistively heated to 2000 K to remove adsorbed oxygen completely and obtain a clean sample. In practice, however, repeated treatment to such high temperatures severely limits the lifetime of such a mounting arrangement, so that the manipulator has been fitted with electron-beam heating. In this case, a tungsten ribbon filament is placed just behind the sample and the sample is raised to a large positive potential ($\sim$500 V) with the filament heated. This allows the sample to be repeatedly heated to 2100 K without any adverse effects on the heating wires. The sample can also be cooled to $\sim$80 K via thermal contact to a liquid-nitrogen filled reservoir. Resistive heating was used to collect temperature-programmed desorption (TPD) data at a heating rate of 10 K s^{-1} and for sample cleaning in oxygen. Temperature-programmed desorption data were collected using a computer-multiplexed quadrupole mass spectrometer which could collect up to five masses sequentially. The sample temperature was also monitored by the computer. In order to avoid ground loops, since the thermocouple is electrically in contact with the metal sample, the thermocouple was electrically isolated from the computer using an opto-isolator so that the output from the thermocouple is converted to frequency and input into a counter in the computer. The analyzer head of the quadrupole was enclosed in an evacuated shroud with a 1 cm-diameter hole in the front to minimize signals not arising from the sample entering the mass spectrometer ionizer. However, in order to further minimize the possibility of interference from desorption from support rods (which was found to be a problem when high methylene iodide doses were used), methylene iodide was dosed directly onto the sample using a 5 mm internal diameter tube directed at the sample. This allowed effects due to desorption from the support rods to be eliminated. The shapes of the TPD curves obtained by this method and by backfilling the chamber were in good agreement, indicating that exposing the Mo(100) surface via the dosing tube led to uniform coverages. The effective doses provided by the tube were calibrated by comparison with temperature-programmed

desorption data obtained by back-filling the chamber, which showed that the tube yielded an approximately 1000-fold increase in methylene iodide dose compared to just pressurizing the chamber.

The chamber was also equipped with a four-grid retarding field analyzer (RFA) which was used to obtain LEED images of the sample and to collect Auger data. The sample was cleaned by heating in $\sim 2.5 \times 10^{-7}$ Torr of oxygen at 1200 K for 5 min to remove carbon and then rapidly heating in vacuo to 2100 K to remove oxygen. This resulted in the diffusion of further carbon to the surface, and this procedure was repeated until no impurities, particularly carbon, were noted in the surface after heating to 2000 K.

Ultraviolet photoelectron spectra were obtained at the Wisconsin Synchrotron Radiation Center using the Aladdin storage ring. The stainless steel, ultrahigh vacuum chamber used for these experiments operated at a base pressure of $\sim 1 \times 10^{-10}$ Torr following bakeout and was attached to the end of a Mark V Grasshopper monochromator. The chamber was equipped with a quadrupole mass analyzer for residual gas analysis and to test gas purities. It also contained a double-pass cylindrical mirror analyzer which was used to collect both Auger and photoelectron spectra. Auger spectra were excited using a 3 keV electron beam and collected by pulse-counting the scattered electrons and the $dn(E)/dE$ Auger spectrum obtained by numerically differentiating the $n(E)$ signal. The analyzer was operated at a pass energy of 25 eV to collect photoelectron spectra and this yielded an overall spectral resolution of 0.15 eV. Photoelectron spectra were excited using 60 eV radiation which has been shown previously to yield the optimum C 2s to background intensity ratio on Mo(100) [54]. Spectra were collected by adding ten separate scans, and the incident beam flux was monitored using a gold grid placed in the path of the beam. Individual spectra were checked for consistency prior to addition to ensure that there was no significant adsorbate degradation due to the photon beam or adsorption of contaminants from the background during data collection. Samples were dosed at 80 K and annealed for 5 s to the desired temperature and allowed to cool to 80 K, following which the spectra were recorded.

The methylene iodide (Aldrich, 99%) was transferred from the bottle into a glass vial which was shrouded in aluminium foil to minimize photochemical decomposition, and purified by repeated freeze–pump–thaw cycles and again stored in glass. Deuterated methylene iodide (Aldrich, 99%) was similarly purified. The oxygen (AGA Gas, Inc., 99%) was transferred from the cylinder to a glass bulb and also redistilled. The gas-handling line was constructed from glass to minimize decomposition after transfer from the bottles to the line. The purity of the gasses was measured using mass spectroscopy by leaking into the UHV portion of the chamber and measuring the spectrum using the quadrupole mass analyzer. No impurities were detected in the oxygen. A small amount (<1%) of methyl iodide was present in the methyl iodide even after the cleaning procedure described above.

Oxygen overlayers were prepared by saturating the Mo(100) surface (20 L O_2 exposure at 1050 K; $1\ L = 1 \times 10^{-6}$ Torr·s) and annealing to various temperatures in order to remove oxygen to obtain the requisite coverage. The adsorption of oxygen on Mo(100) has been studied very extensively, and the oxygen coverages were calibrated from their characteristic LEED patterns [45–52] and confirmed from their relative O/Mo Auger ratios (by monitoring the O KLL and Mo LMM Auger transitions).

3. Results

Shown in Fig. 1 are a series of ultraviolet photoelectron spectra obtained as a function of sample annealing temperature after the exposure of clean Mo(100) to 10 L of methylene iodide with the sample initially at 80 K. The exposures quoted are uncorrected for ionization gauge sensitivities. Emission intensity from within a few eV of the Fermi level (indicated as 0 eV binding energy) is associated with emission from the substrate d-bands, and the large background is due to inelasticly scattered electrons. Features above ~3 eV binding energy are due to the presence of adsorbed methylene iodide since this region is featureless for

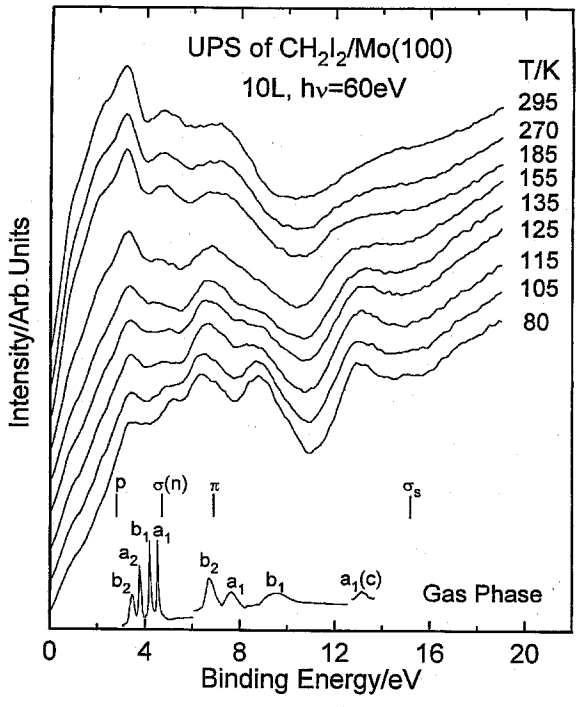

Fig. 1. Ultraviolet photoelectron spectra of methylene iodide adsorbed on Mo(100) (10 L) at a sample temperature of 80 K. The sample was heated to the temperature indicated adjacent to each spectrum for a period of 5 s and allowed to cool to 80 K following which the spectrum was recorded. Spectra were obtained using 60 eV photons. Shown for comparison is the gas-phase ultraviolet photoelectron spectrum for methylene iodide and the positions of the energy levels calculated for adsorbed CH_2 using Hückel theory.

clean Mo(100). Shown for comparison is the gas-phase spectrum of methylene iodide, which has been uniformly shifted so that the peaks align [55] to compensate for the different reference levels used for gas-phase and surface spectra (vacuum versus Fermi levels) and any initial- and final-state effects. The agreement between the peak positions in the spectrum for methylene iodide on Mo(100) at 80 K and the gas-phase spectrum is good, indicating that methylene iodide adsorbs molecularly at this temperature. This spectrum exhibits peaks at 13.2, 9.0, 7.4, 6.4 and 3.4 eV binding energy which are assigned to the presence of molecularly adsorbed methylene iodide (see below). As the sample is heated, the shape of the spectrum changes considerably, indicating the decomposition of the methylene iodide on the surface, in particular from the decrease in intensity of the 9.0 eV feature. This peak is completely absent after annealing the sample to ~185 K when the spectrum then consists of peaks at ~13, ~7, 4.7 and 3.1 eV binding energy. The assignment of these features will be discussed in greater detail below. Note, however, that the temperature range over which the spectral changes take place are in good agreement with the temperature at which methylene iodide is found to thermally decompose to form adsorbed CH_2 species and iodine on Mo(110) using surface infrared spectroscopy [44].

Fig. 2 shows a series of thermal desorption spectra obtained after 10 L exposure of Mo(100) to d_2-methylene iodide. A small amount of deuterated methane (18, 20 amu) desorption is detected at ~240 K, and the formation of methane is confirmed by comparison of the mass spectral fragmentation pattern with the integrated desorption yield obtained in temperature-programmed desorption at various masses. The origin of the

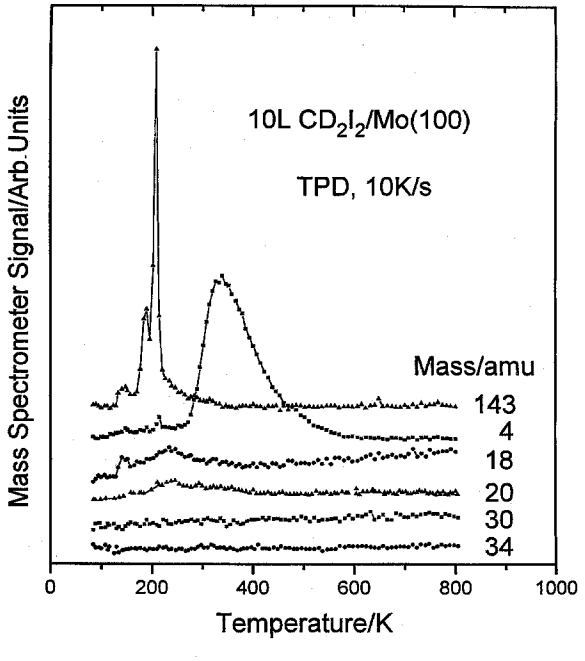

Fig. 2. Temperature-programmed desorption spectra of d_2-methylene iodide (10 L) from Mo(100) showing the desorption of hydrogen (4 amu), methane (18, 20 amu), methylene iodide (143 amu), ethylene (30 amu) and ethane (34 amu).

methane will be discussed in greater detail below. Deuterium (4 amu) desorption is also found at ~350 K and, in addition, the desorption of molecular methylene iodide (143 amu) is found at these high exposures at ~205 K. This peak is assigned to the formation of second-layer methylene iodide, since it continues to grow with increasing exposure without showing any signs of saturating. No other iodine-containing species are detected. The amount of molecular methylene iodide at this exposure accounts for only (<10%) of the surface species. 30 amu (ethylene) and 34 amu (ethane) traces are also shown on this spectrum and indicate that neither ethylene nor ethane are formed.

Shown in Fig. 3 are a series of temperature-programmed desorption spectra of methylene iodide (3 L) adsorbed onto a hydrogen pre-covered surface as a function of hydrogen exposure. These results show that the amount of methane desorbing from the surface increases with increasing hydrogen coverage, implying that methane is formed by the reaction of hydrogen with methylene species formed by methylene-iodide decomposition. In addition, the peak shifts to lower temperature as the hydrogen coverage increases implying a second-order reaction. Note that no methane desorption is detected while dosing the surface with methylene iodide. In order to further confirm the source of the hydrogen in the formation of methane, a deuterium-covered surface (5 L exposure) was exposed to CH_2I_2 (5 L). The results are displayed in Fig. 4. No CD_4 (20 amu) or CHD_3 (19 amu) are detected, and the maximum number of deuteriums incorporated into the reactively formed methane is two. This result indicates that methane is formed by the reaction of an adsorbed CH_2 species with surface deuterium. It should be noted that these peaks are not due to the desorption of water. This result is confirmed since no water is found to desorb from hydrogen adsorbed on oxygen-covered Mo(100), in agreement with the results of other workers [56].

Fig. 5 displays the results of varying the initial

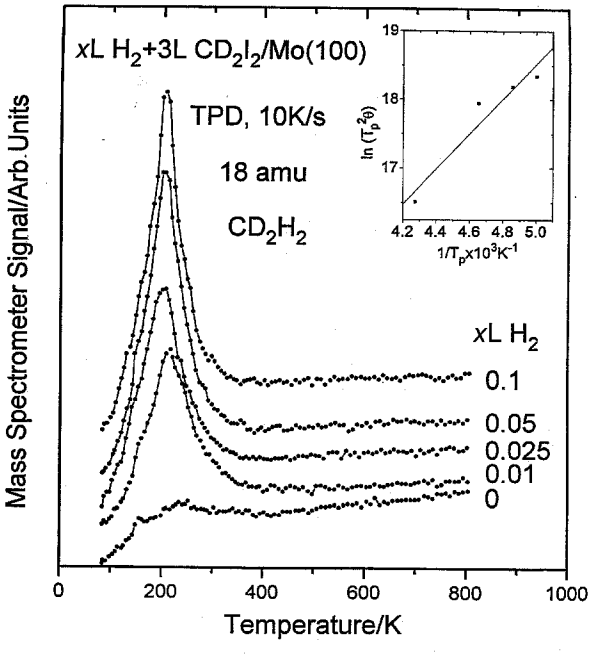

Fig. 3. Temperature-programmed desorption spectra of methane (18 amu) from the coadsorption of hydrogen and d_2-methylene iodide on Mo(100) as a function of hydrogen exposure. Shown as an inset is a plot of $\ln(T_p^2\theta)$ versus $1/T_p$ taken from these data, giving an activation energy of 21 ± 1 kJ mol^{-1}.

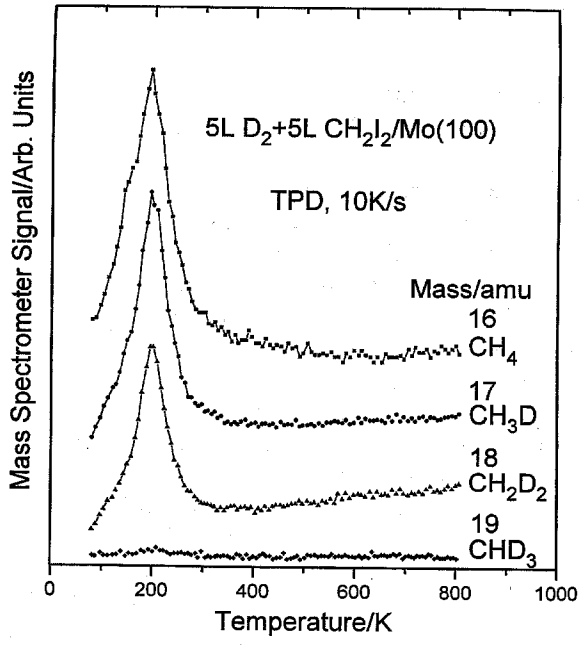

Fig. 4. Temperature-programmed desorption spectra collected at various masses following adsorption of CH_2I_2 (5 L) on Mo(100) precovered by deuterium (5 L) at 80 K.

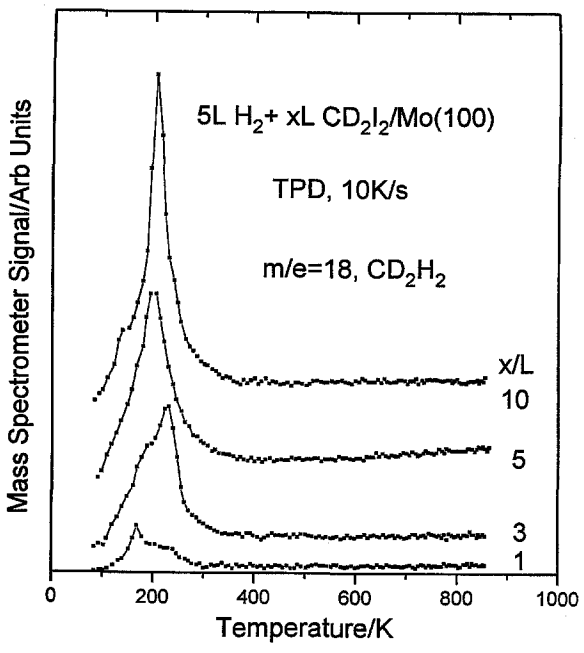

Fig. 5. Temperature-programmed desorption spectra of methane (18 amu) from the coadsorption of hydrogen and d_2-methylene iodide on Mo(100) as a function of methylene iodide exposure.

d_2-methylene iodide exposure to a hydrogen-precovered (5 L H_2) Mo(100) surface. Again, the methane yield increases with increasing methylene iodide exposure and the peak temperature also decreases as the exposure increases, indicating an associative reaction between adsorbed CD_2 and hydrogen. The origin of the small desorption state at $\sim$170 K for low d_2-methylene iodide exposures is not known, but may be due to reactions at defects.

Finally, since such C_1 species have been proposed to polymerize to form higher hydrocarbons on transition-metal surfaces [1–13], an attempt was made to detect ethylene or ethane desorption. Carbene coupling has been found in ultrahigh vacuum on copper [57], and carbon–carbon bond formation has been detected on iron from the interaction of CO and diazomethane [58]. Methyl coupling has been found on silver [51] and copper [57,60], and carbene dimerization to acetylene has been seen on Ni(111) [60]. However, as shown in Fig. 2, no ethylene or ethane desorption were detected from Mo(100).

Various oxygen overlayers of different coverages were obtained by annealing an oxygen-saturated $p(1\times1)$ surface to various temperatures. These consisted of a (2×1) surface obtained by annealing at 1600 K to yield an oxygen coverage $\theta_O=$ 1.1 ML, a $(\sqrt{5}\times\sqrt{5})$ pattern producing an oxygen coverage $\theta_O=0.83$ ML and a (4×4) surface giving $\theta_O=0.2$ ML. These LEED patterns reproduced those found by other workers [45–52]. Finally, the relative oxygen coverages were checked by measuring the O/Mo Auger ratio as a function of annealing temperature. The resulting plot of oxygen Auger ratio as a function of annealing temperature is displayed in Fig. 6, which reveals a smooth decrease in coverage as a function of annealing temperature. Plotted on the right ordinate are the oxygen coverages calibrated from the LEED patterns which shows that coverages between 1.35 and 0.2 monolayers can be obtained merely by annealing to various temperatures.

Figs. 7–9 display photoelectron spectra from methylene iodide adsorbed on oxygen-covered Mo(100) at different oxygen coverages. Again, the overlayer spectra are compared with the gas-phase spectrum [55] and these results show that methylene iodide adsorbs molecularly at 80 K on these surfaces. Displayed as "clean" are the spectra of oxygen alone on Mo(100). Note also that the relative intensity of the adsorbate signals decreases with increasing oxygen coverage, so that the amount of methylene iodide that can be accommodated onto the surface decreases with increasing oxygen coverage (see below). In all cases, as the sample is heated to $\sim$180 K the form of the spectrum changes, connoting chemical decomposition of the adsorbate eventually leading to peaks at 12.6, 7.0, 4.7 and 3.3 eV binding energy on the 0.2 ML oxygen surface (Fig. 7). Note that the peak at 7.0 eV binding energy has contributions from emission from the oxygen 2p levels. Peaks are evident at 13.0, 7.0, 4.7 and 3.2 eV binding energy on the 0.83 ML O surface (Fig. 8), and again the 6.8 eV peak position is uncertain since it contains contributions from the adsorbed oxygen. The oxygen peak is clearly evident in the 1.35 mono-

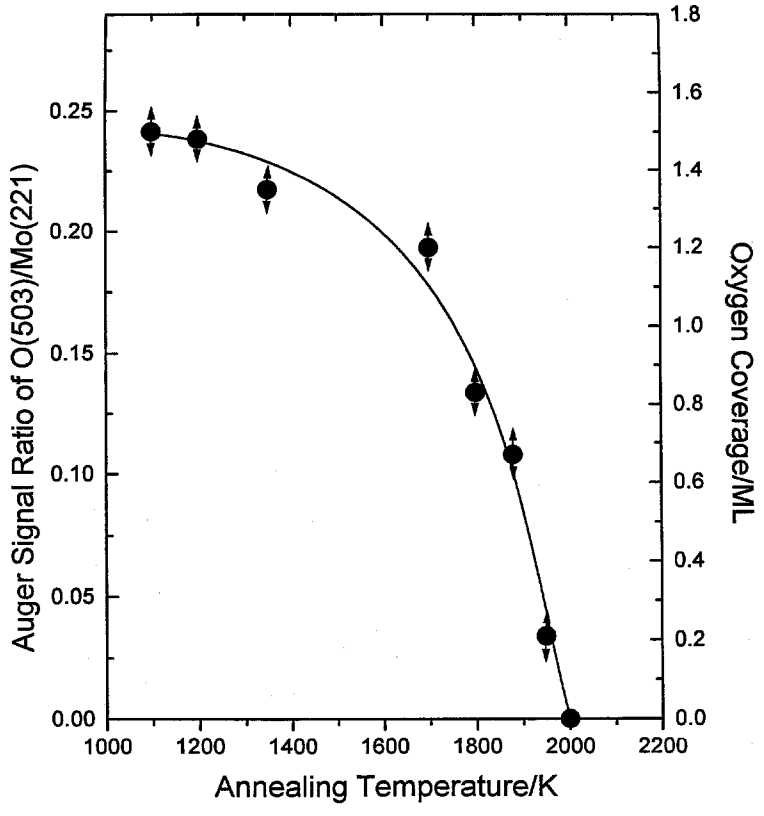

Fig. 6. Plot of oxygen/molybdenum Auger ratios for oxygen overlayers on Mo(100) as a function of annealing temperature. The corresponding oxygen coverages are displayed on the right-hand ordinate.

layer oxygen surface (Fig. 9) as a broad feature at 4 and 8 eV binding energy.

Fig. 10 displays the deuterium (4 amu) temperature-programmed desorption spectra obtained following saturation of O/Mo(100) surfaces with d_2-methylene iodide as a function of increasing oxygen coverage. Two trends are notable in this case. First, the total deuterium yield decreases as a function of increasing oxygen coverage, and second, the desorption peak temperature increases with increasing oxygen coverage. For comparison, shown in Fig. 11 are a series of deuterium (4 amu) desorption spectra after dosing oxygen-covered Mo(100) with deuterium itself, displayed as a function of oxygen coverage.

Fig. 12 shows the corresponding methane thermal desorption spectra as a function of oxygen coverage obtained by dosing various oxygen-precovered surfaces with hydrogen and then adsorbing d_2-methylene iodide. The methane formation kinetics are only slightly affected by the presence of oxygen where the peak temperature varies from 205 K for clean Mo(100) to ~300 K for $\theta_O = 1.35$. The total desorption yield also decreases rapidly with oxygen coverage. Once again, measurement of the fragmentation pattern of the desorbing species on various oxygen-covered surfaces reveals the incorporation of a maximum of two hydrogens in the reactively formed methane in all cases.

4. Discussion

4.1. Methylene iodide adsorbed on Mo(100)

The photoelectron spectrum of methylene iodide adsorbed on Mo(100) at 80 K (Fig. 1) clearly

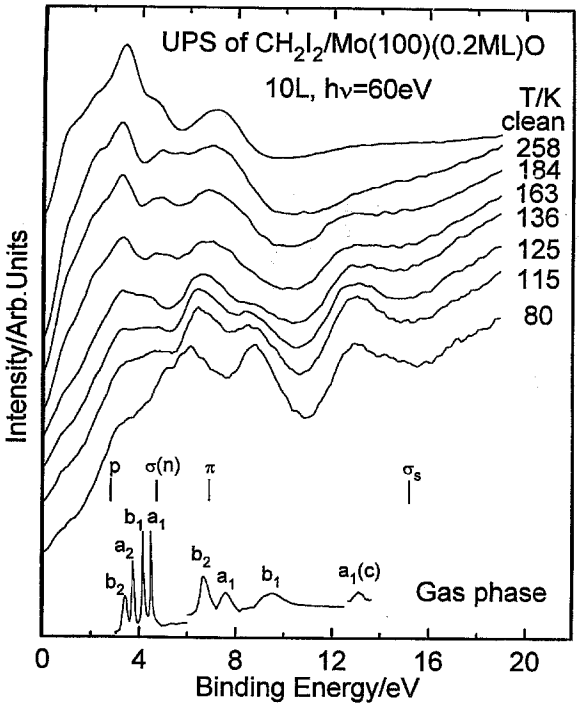

Fig. 7. Ultraviolet photoelectron spectra on methylene iodide adsorbed on O/Mo(100) (10 L) at a sample temperature of 80 K. The oxygen coverage is 0.2 ML. The sample was heated to the temperature indicated adjacent to each spectrum for a period of 5 s and allowed to cool to 80 K, following which the spectrum was recorded. Spectra were obtained using 60 eV photons. Shown for comparison is the gas-phase ultraviolet photoelectron spectrum for methylene iodide and the positions of the energy levels calculated for adsorbed CH_2 using Hückel theory.

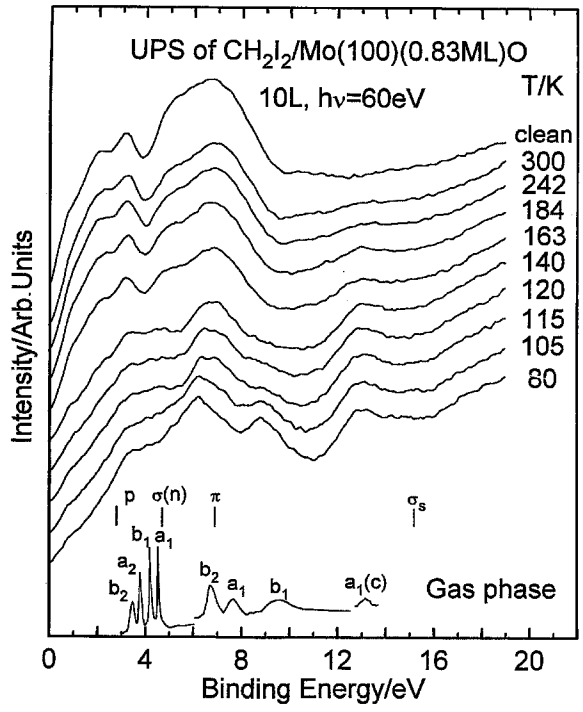

Fig. 8. Ultraviolet photoelectron spectra on methylene iodide adsorbed on O/Mo(100) (10 L) at a sample temperature of 80 K. The oxygen coverage is 0.83 ML. The sample was heated to the temperature indicated adjacent to each spectrum for a period of 5 s and allowed to cool to 80 K, following which the spectrum was recorded. Spectra were obtained using 60 eV photons. Shown for comparison is the gas-phase ultraviolet photoelectron spectrum for methylene iodide and the positions of the energy levels calculated for adsorbed CH_2 using Hückel theory.

indicates the presence of adsorbed molecular methylene iodide at this temperature. Temperature-programmed desorption data (Fig. 2) indicate that unreacted methylene iodide desorbs at ~200 K but accounts for only ~10% of the surface after a 10 L exposure, so that the photoelectron spectra exhibit features predominantly due to the adsorbed overlayer. The peak positions at this temperature agree well with the gas-phase spectrum of methylene iodide [55] where the peaks are assigned as 13.2 (a_1 due to C 2s orbitals), 9.0 (b_1), 7.4 (b_2), 6.4 (a_1) and 3.4 (a_1, a_2, b_1, b_2) eV binding energy. The shape of the spectrum changes considerably on annealing the sample, and is particularly manifest by the attenuation in intensity of the 9.0 eV peak, which has completely disappeared on heating to ~180 K. At this point, the spectrum is characterized by features at 13, 7, 4.7 and 3.1 eV. It has also been shown using infrared spectroscopy that methylene iodide thermally decomposes on Mo(110) to yield an adsorbed methylene species [44] and deposit chemisorbed iodine on the surface. A similar assignment is made for the spectral transformations observed in ultraviolet photoelectron spectroscopy in this case. In order to confirm this, and to assign the peaks observed in the 185 K spectra, an extended Hückel calculation was performed for a methylene species coordinated to a molybdenum metal cluster adsorbed on a bridge site on a Mo(100) surface [62]. While this

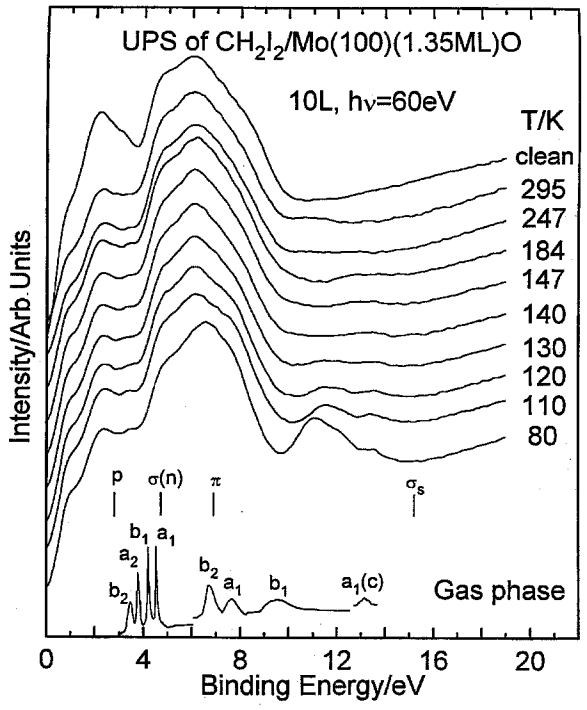

Fig. 9. Ultraviolet photoelectron spectra on methylene iodide adsorbed on O/Mo(100) (10 L) at a sample temperature of 80 K. The oxygen coverage is 1.35 ML. The sample was heated to the temperature indicated adjacent to each spectrum for a period of 5 s and allowed to cool to 80 K, following which the spectrum was recorded. Spectra were obtained using 60 eV photons. Shown for comparison is the gas-phase ultraviolet photoelectron spectrum for methylene iodide and the positions of the energy levels calculated for adsorbed CH_2 using Hückel theory.

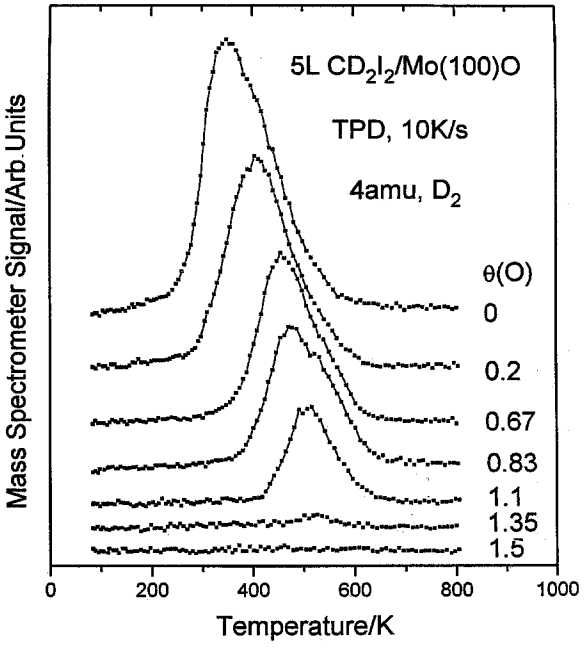

Fig. 10. Plot of the deuterium (4 amu) thermal desorption spectra from d_2-methylene iodide (5 L) adsorbed onto O/Mo(100) as a function of oxygen coverage. Oxygen coverages are indicated adjacent to the corresponding spectrum.

is not an accurate calculation, since the parameters used in establishing ionization energies are based on the ionization potentials for each of the atomic levels, it should lead to a reasonable correspondence between the observed and calculated species. The results are summarized in Fig. 13, which indicates the ionization potentials of the levels and the form of the molecular orbitals. The results yield an ionization energy of the σ_s level (a_1 symmetry) of 24.06 eV, of the π-CH_2 level (b_1 symmetry) of 15.79 eV, of the σ(n) level (a_1) of 13.63 eV and of the p level (b_2) of 11.69 eV. The position of these levels are also marked on the spectra in Fig. 1, where the binding energies have been shifted uniformly to align with the observed levels. The agreement between the calculated and experimental results for an adsorbed CH_2 species is remarkably good, except for the σ_s state where the calculated energy is substantially higher than the measured value. This allows the features in the spectrum obtained after annealing to 185 K to be assigned to an adsorbed carbene as: 13 eV (a_1), 7 eV (b_1), 4.7 eV (a_1) and 3.1 eV (b_2). Bonding to the surface is therefore via donation of electrons from the metal into the b_2 level at 3.12 eV binding energy. Hückel calculations predict that the lowest unoccupied anti-bonding level is some 15 eV above the Fermi level [62], so that back-donation into these levels only contributes in a very minor way to the bonding at the surface which is therefore primarily via donation of metal electrons into the vacant p orbitals at ~3 eV below the Fermi level. This indicates that the adsorbed carbene should carry a substantial negative charge, and Hückel calculations for carbenes adsorbed on small metal clusters confirm this [62].

The ionization energy in the photoelectron

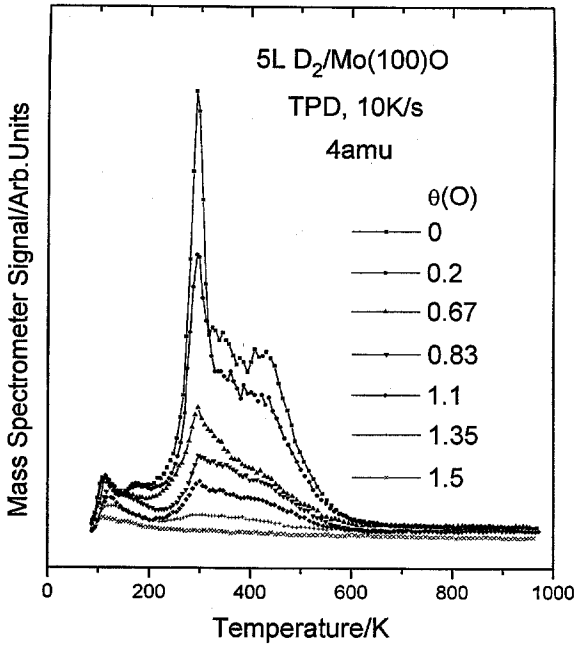

Fig. 11. Deuterium temperature-programmed desorption spectra from O/Mo(100) as a function of oxygen coverage.

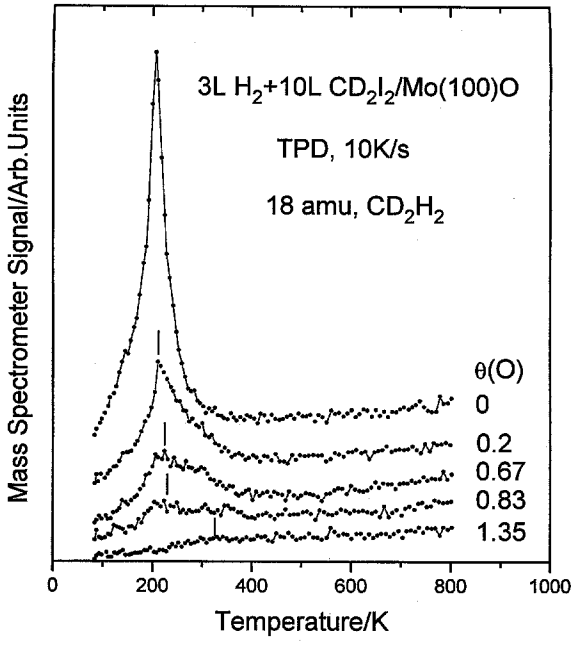

Fig. 12. Plot of the methane thermal desorption spectra from d_2-methylene iodide (10 L) adsorbed onto O/Mo(100) precovered with hydrogen (3 L) as a function of oxygen coverage. Oxygen coverages are indicated adjacent to the corresponding spectrum.

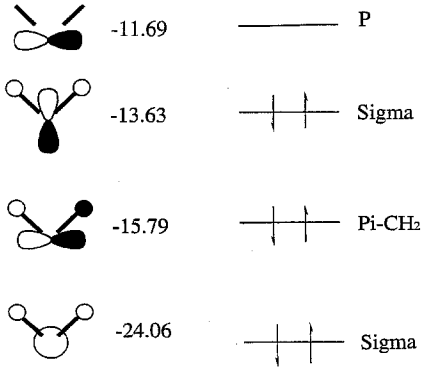

Fig. 13. A diagram showing the orbitals and their ionization energies for a CH_2 species on molybdenum calculated using Hückel theory.

spectrum can be used to estimate Mulliken electronegativities. For the substrate, this is simply the work function, ϕ, and, for the adsorbed carbene from the binding energies of the p and σ orbitals, is $\phi+3.8$. The difference in Mulliken electronegativities for the carbene and the surface, $\Delta\chi_M$, is therefore 3.8. This is directly related to the Pauling electronegativity by a factor of 3.15 [63], yielding a Pauling electronegativity difference $\Delta\chi_P$ of 1.24. This implies that the carbene–metal bond has a dipole moment of $\sim$1.24 D and that the bond possesses $\sim$25% ionic character, in accord with the results of the Hückel calculations referred to above [62]. Note that the substrate work-function is likely to be modified by the presence of oxygen and iodine. The electronegativity difference is unaffected by changes in this value.

The data of Fig. 2 illustrate that the major reactively desorbing species following methylene iodide adsorption are methane and hydrogen. The results in Fig. 11 show that deuterium desorbs from a Mo(100) surface in three states at $\sim$295, 350 and 420 K, whereas deuterium from adsorbed CD_2 desorbs in a single state at $\sim$350 K. From the desorption peak temperature of $\sim$350 K, a simple Redhead analysis [64] yields an activation energy for dehydrogenation of $\sim$90 kJ mol^{-1} using a heating rate of 10 K s^{-1} and a typical pre-exponential factor of 1×10^{13} s^{-1}.

Methane desorbs at a sample temperature of ~240 K, which is substantially lower than that at which the adsorbed species dehydrogenates (~350 K), which suggests that adsorbed methylene species cannot supply the requisite hydrogen except via a direct hydrogen transfer between adsorbed species. In order to establish the origin of the hydrogen required for methylene hydrogenation, the surface was pre-dosed with deuterium (D_2), and methylene iodide (CH_2I_2) adsorbed onto the surface and TPD spectra collected (Fig. 4). A similar 200 K peak is detected, but with a much increased intensity compared to adsorbing methylene iodide alone, and the major desorbing species is d_2-methane with no d_3- or d_4-products. This indicates that the adsorbed methylene reacts with adsorbed hydrogen to yield methane rather than directly with another CD_2 species. These results are also in accord with the assignments made from photoelectron spectroscopic data that an adsorbed CD_2 (CH_2) species is formed by reaction of methylene iodide, and that this reacts without any intervening exchange with surface hydrogen, to yield methane. This result is emphasized by the data of Fig. 3, which displays the methane (18 amu, CD_2H_2) TPD spectrum as a function of hydrogen exposure and after subsequently exposing the surface to 3 L of CD_2I_2. There is clearly a substantial increase in the amount of methane evolved from the surface. The small amount of methane found without intentionally pre-adsorbing hydrogen is probably partly due to hydrogen adsorption from the background, with perhaps a small contribution from carbene dehydrogenation. Note in addition that there is a shift in peak temperature to lower values as the hydrogen coverage increases, indicative of a second-order reaction. An activation energy for the reaction can be found from a plot of $\ln(T_p^2\theta)$ versus $1/T_p$ [64], where θ is calculated from the area of the desorption peak and is shown as an inset in Fig. 3. This yields a relatively low value of activation energy of 21 ± 2 kJ mol^{-1}, consistent with the relatively low desorption peak temperature of ~200 K.

The results of a similar experiment, in which the hydrogen coverage is kept constant but where the methylene iodide exposure is varied, is shown in Fig. 5. In this case, there is a similar increase in desorption yield and a concomitant decrease in peak temperature, consistent with a reaction between adsorbed hydrogen and a carbene. The formation of methane from methylene iodide must proceed via a methyl intermediate. It is not known from the results presented here whether the addition of the first hydrogen to form a methyl species or the addition of hydrogen to this species to yield methane is rate-limiting. Probing the methane-formation kinetics by hydrogenating methyl species formed from methyl iodide on oxygen-modified Mo(100) should provide information on these relative reaction rates.

It should be noted that no carbon–carbon coupling reactions were observed on Mo(100), since no ethylene or ethane were detected (Fig. 2). However, it has been proposed that this can occur catalytically at higher pressures, but with a relatively large activation energy of ~65 kcal mol^{-1} [32,33]. Photoelectron spectroscopic results imply that firstly, the C–metal bond should be rather strong and secondly, that the carbenes should be negatively charged, both of which would mitigate against coupling reactions on the surface.

These results can be used to estimate approximate values for the heat of adsorption of the carbene, $\Delta H_{ads}(CH_2)$. The activation energy for methane formation, $E(CH_4)$, is given by:

$$E(CH_4) \approx \Delta H_{ads}(CH_2) + 2\Delta H_{ads}(H) - D(CH_2\text{–}H) - D(CH_3\text{–}H), \quad (1)$$

where $\Delta H_{ads}(H)$ is the heat of adsorption of hydrogen (~60 kcal mol^{-1} [65]), $D(CH_2\text{–}H)$ is the bond strength of the CH_2–H bond (111 kcal mol^{-1} [66]) and $D(CH_3\text{–}H)$ is the strength of the CH_3–H bond (104 kcal mol^{-1} [66]). Using the activation energy to methane formation measured above, this yields a value of $\Delta H_{ads}(CH_2)$ of ~100 kcal mol^{-1}.

Similarly, the activation energy of carbene recombination can be approximated as

$$E(C_2H_4) \approx 2\Delta H_{ads}(CH_2) - D(C{=}C), \quad (2)$$

where $E(C{=}C)$ is the carbon–carbon bond strength in ethylene (173 kcal mol^{-1} [66]). This yields $\Delta H_{ads}(CH_2) \approx 120$ kcal mol^{-1}.

4.2. Effect of oxygen on methylene iodide adsorbed on Mo(100)

The data of Fig. 6 show that relatively large coverages of oxygen (up to ~1.5 monolayers) can be accommodated onto a Mo(100) surface. The coverages obtained at various sample annealing temperatures are measured using Auger spectroscopy, and these are calibrated by the array of LEED patterns exhibited by the surface [45,52].

The vacant oxygen 2p acceptor levels are located at about 6 eV below the Fermi level (see, for example, Fig. 8) and have the effect of oxidizing the surface molybdenum atoms. The surface oxidation state has been measured using X-ray photoelectron spectroscopy, where it is shown that surface molybdenum oxidation states of up to +4 can be achieved using oxygen overlayers [67]. This can also be seen in the effect of oxygen on the work-function change of a Mo(100) surface, which increases by 1.1 V for an oxygen coverage of 1.35 monolayers. Interestingly, the work function initially decreases as the oxygen coverage increases to 0.2 monolayers [52]. A priori, it can be anticipated that this will decrease the binding energy of adsorbate levels of the adsorbed carbene.

Fig. 7 displays the photoelectron spectra for methylene iodide adsorbed on Mo(100)+ 0.2 ML O. The spectral changes observed in this case are essentially identical to those found for methylene iodide on Mo(100) (Fig. 1). Methylene iodide adsorbs molecularly at 80 K, and the adsorbate-induced spectrum agrees well with that for gas-phase methylene iodide. The 8.8 eV binding energy (b_1) feature attenuates on heating the sample and is completely absent after annealing at ~160 K, connoting thermal decomposition of the methylene iodide. The positions of the carbene peaks from the Hückel calculations described above [62] are also marked on the spectrum, indicating that a carbene is also formed on this surface. Note that the presence of emission from the adsorbed oxygen partially obscures the 7 eV (b_1) carbene peak. Similar spectral changes are noted for methylene iodide adsorption on a Mo(100) surface covered with 0.83 ML of oxygen (Fig. 8), where the molecular species decomposes on annealing to ~140 K and the positions of the carbene peaks from Hückel theory are also marked. The relative intensity of the oxygen peak increases with increasing oxygen coverage.

The positions of the molecular peaks are shifted substantially as the oxygen coverage increases to 1.35 monolayers (Fig. 9), and in this case the a_1 peak has a binding energy of ~11 eV, as illustrated by the corresponding gas-phase spectrum. The peak at 2.3 eV binding energy found after heating the surface to above 130 K is assigned to the p peak of b_2 symmetry of the carbene. Support for this assignment comes from the data displayed in Table 1. This compares the shift in position of the p (b_2) peak, which is fairly sharp and can be measured quite accurately, with the change in work function (taken from Ref. [52]). Clearly, except for the result for $\theta_O = 0.83$, the correlation between the shift in the position of this peak and the work-function change is good. Note that the surface is proposed to reconstruct for an oxygen coverage of 0.83 (where it exhibits a $(\sqrt{5} \times \sqrt{5})$ LEED pattern [45–51]). The data indicate, however, that this peak can consistently be assigned to the same level for the carbene, and that its location is affected by the presence of oxygen on the surface.

Fig. 10 displays a series of deuterium thermal desorption spectra following a 5 L exposure to various oxygen-covered Mo(100) surfaces with d_2-methylene iodide. As noted above, the total integrated intensities of the peaks decrease with increasing oxygen coverage, reflecting the paucity of sites available for adsorption as the oxygen coverage increases. This will be discussed in greater detail below. In addition, the peak temperature increases with increasing oxygen coverage, and the data of

Table 1
Comparison of the work-function change of a Mo(100) surface with shifts in the binding energy of the carbene π^*-CH_2 antibonding level

θ_O	$E_B(b_2)$ (eV)	$\Delta\phi$	ΔE_B (eV)
0	3.10	0	0
0.2	3.35	−0.2	−0.25
0.83	3.30	+0.8	−0.2
1.35	2.30	+1.1	+0.8

Fig. 11 illustrate that adsorbed deuterium evolves from the surface with completely different profiles to those measured for the carbene-covered surface (Fig. 10). This indicates, as was found for CD_2/Mo(100), that deuterium formation is decomposition- rather than desorption-rate limited, and implies that the decomposition activation energy increases with increasing oxygen coverage. This effect is illustrated in Fig. 14, which plots the activation energies for deuterium formation from CD_2 decomposition calculated using the Redhead equation [64] versus oxygen coverage, showing that the activation energy varies from ~ 90 kJ mol^{-1} for clean Mo(100) to ~ 130 kJ mol^{-1} for an oxygen coverage of 1.35 monolayers; oxygen has a substantial effect on the decomposition kinetics. The results of Hückel calculations show that the C–H overlap population varies only slightly with a change in the nature (and work function) of the metal [62]. This effect can be rationalized since the vacant p molecular orbital of the carbene which predominantly participates in bonding is essentially non-bonding with respect to hydrogen (Fig. 13), so that the substantial change in decomposition kinetics cannot be directly related to a modification of the C–H bonds in the adsorbed carbene. This phenomenon must therefore be ascribed to the effect of adsorbed oxygen on the transition state to decomposition. However, it is clear that one of the effects of adsorbed oxygen on the chemistry of the carbene is to stabilize it as the oxygen coverage increases.

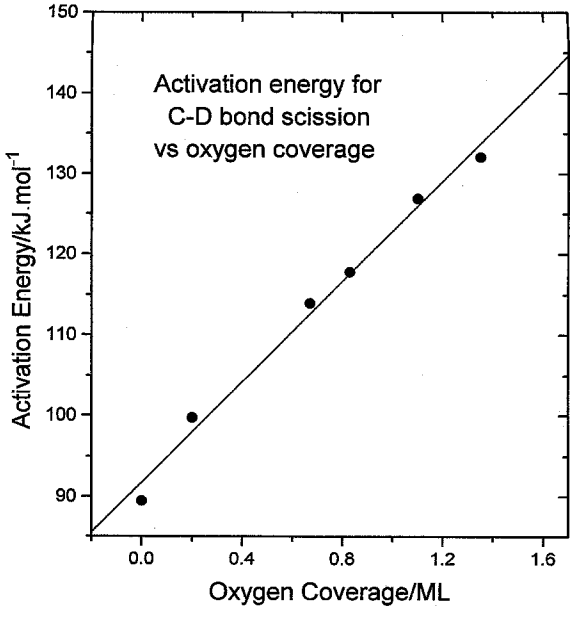

Fig. 14. Plot of the activation energy for carbene decomposition plotted versus oxygen coverage taken from the data of Fig. 10.

Fig. 12 displays the d_2-methane TPD spectra (18 amu) obtained after exposing the oxygen-covered Mo(100) surface to hydrogen and then to d_2-methylene iodide. Again, measurement of the fragmentation patterns of the reactively formed methane indicates that a maximum of two hydrogens are incorporated into the molecule, as was found on Mo(100). The amount of methane decreases drastically with increasing oxygen coverage, indicating that sites for the adsorption and decomposition of methylene iodide are blocked by oxygen. In addition, there is a slight increase in the peak maximum as the oxygen coverage increases. In this case, it would be anticipated that increasing the work function of the Mo(100) by adding oxygen would have the effect of decreasing the carbene binding energy since the adsorbed oxygen competes with the carbene for electrons. As shown from Eq. (1), this would a priori be expected to manifest itself in a decrease in activation energy to methane formation as the oxygen coverage increases. In addition, the negative charge on the carbene would also be expected to decrease with increasing oxygen coverage, facilitating reaction between the carbene and adsorbed hydrogen. However, an additional effect of the addition of oxygen to the surface on the methane formation kinetics is to decrease the hydrogen and carbene coverages. The lower hydrogen and carbene coverages will correspondingly increase the desorption temperature for methane formation in TPD. In order to attempt to gauge the extent of this effect, the predicted peak positions for each of the methane desorption yields, (measured from the area under the TPD curves, Fig. 12) are calculated using the kinetic parameters for methane formation on clean Mo(100) (Fig. 4) [64], and the resulting peak temperatures are marked as vertical lines on the data of Fig. 12. Interestingly these agree rather well with the experimental peak positions for the oxygen-covered surfaces, indicating that an

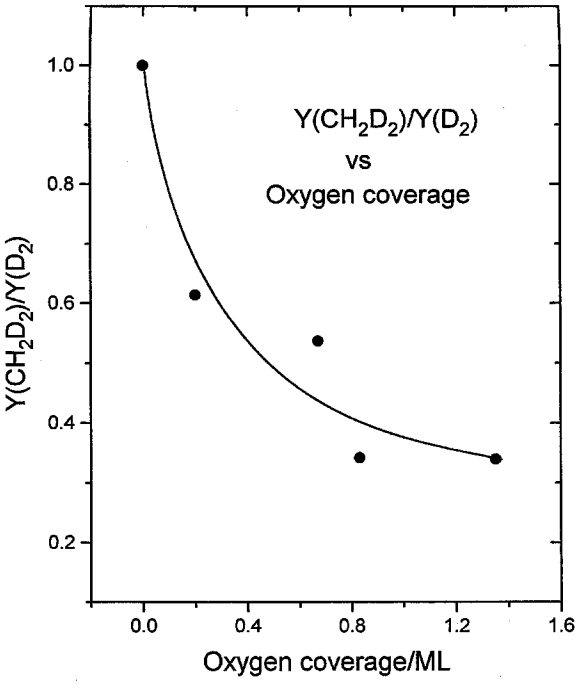

Fig. 15. Plot of the ratio of the methane yield to the yield of hydrogen, $Y(CH_2D_2)/Y(D_2)$ for methylene iodide adsorbed on oxygen-covered Mo(100) as a function of the oxygen coverage.

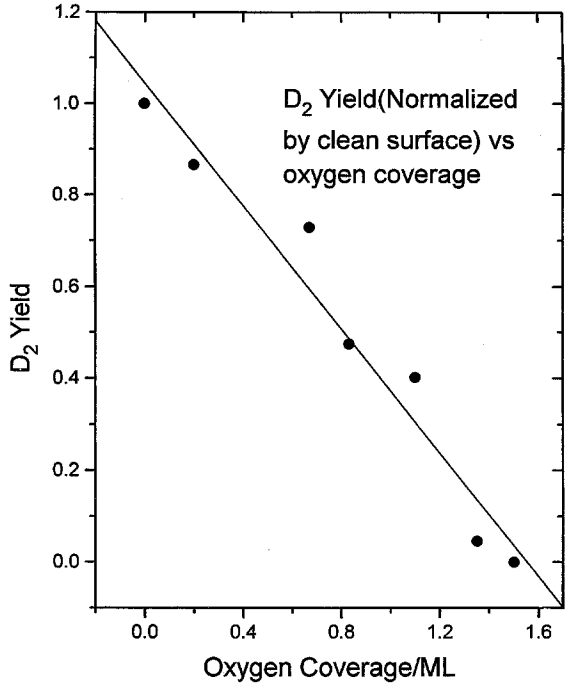

Fig. 16. Plot of the total deuterium yield for d_2-methylene iodide adsorbed on oxygen-covered Mo(100) as a function of oxygen coverage.

adsorbed oxygen overlayer has only a very slight, if any, effect of the methane formation kinetic parameters.

Clearly both the methane (Fig. 12) and hydrogen (Fig. 10) desorption yields decrease with increasing oxygen coverage. Plotted in Fig. 15 is the ratio of the methane and hydrogen yields ($Y(CH_2D_2)/Y(D_2)$) as a function of oxygen coverage normalized to the corresponding ratio for Mo(100). This indicates that the relative methane yield decreases substantially with increasing oxygen coverage and, in spite of the fact that adsorbed methylene species are stabilized by adsorbed oxygen (Fig. 10), this does not lead to a corresponding increase in methane formation.

In the absence of hydrogen, the majority of the adsorbed methylene species dehydrogenate (Fig. 2) so that the integrated yield of hydrogen (D_2) following methylene-iodide adsorption (Fig. 10) merely reflects the saturation carbene coverage for each oxygen coverage. This relative D_2 yield is plotted versus oxygen coverage in Fig. 16, revealing a linear dependence suggesting a direct site-blocking of adsorbed methylene iodide by oxygen.

It might be anticipated also that a decrease in carbene binding energy and charge density at the carbon would have the effect of lowering the activation energy of carbene recombination to form ethylene or ethane (if this hydrogenates rapidly). However, no evidence was found in temperature-programmed desorption for ethylene formation on oxygen-covered Mo(100). Note, however, in catalytic reactions with ethylene which has been proposed to dissociate to yield carbene species, the recombination probability for forming higher hydrocarbons was found to increase with increasing oxygen coverage [39].

5. Conclusions

Methylene iodide decomposes on Mo(100) and on oxygen-covered Mo(100) to form adsorbed

carbenes and deposit iodine. The adsorbed carbene can either react with chemisorbed hydrogen to form methane or thermally decompose to yield hydrogen. Experiments using isotopically labelled reactants demonstrates that methane is indeed formed by the reaction of CH_2 with chemisorbed hydrogen. The carbene thermal decomposition activation energy increases from 90 to $\sim 130\ kJ\ mol^{-1}$ as the oxygen coverage increases to 1.35 monolayers, a phenomenon that is ascribed to the effect of oxygen on the transition state. Pre-adsorbed oxygen blocks sites for both hydrogen and carbene adsorption. However, the methane-formation kinetics do not appear to be affected by the presence of oxygen overlayers, and changes in the methane TPD peak temperature can be ascribed to the effect of site blocking as the oxygen coverage increases.

Acknowledgements

We gratefully acknowledge support of this work by the US Department of Energy, Division of Chemical Sciences, Office of Basic Energy Sciences, under Grant No. DE-FG02-92ER14289. This work is based upon research conducted at the Synchrotron Radiation Center, University of Wisconsin–Madison, which is supported by the NSF under Award No. DMR-95-31009.

References

[1] D.W. Goodman, J. Vac. Sci. Technol. 20 (1982) 522.
[2] D.W. Goodman, R.D. Kelley, T.E. Madey and J.T. Yates, Jr., J. Catal. 63 (1980) 226.
[3] D.W. Goodman, R.D. Kelley, T.E. Madey and J.M. White, J. Catal. 64 (1980) 479.
[4] T. Yamamoto, J. Chem. Soc., Chem. Commun. 1003 (1978).
[5] C.B. Young and G.N. Whiteside, J. Am. Chem. Soc. 100 (1978) 5808.
[6] V. Ponec and W.A.A. Barneveld, Ind. Eng. Chem. Prod. Res. Dev. 18 (1979) 268.
[7] P. Biloen, J.N. Helle and W.H.M. Sachtler, J. Catal. 58 (1979) 95.
[8] R.C. Brady and R.J. Pettit, J. Am. Chem. Soc. 102 (1981) 6181.
[9] R.C. Brady and R.J. Pettit, J. Am. Chem. Soc. 103 (1981) 1287.
[10] W.A.A. Van Barneveld and V. Ponec, J. Catal. 88 (1984) 382.
[11] A.J. Bridgewater, R. Burch and P.C.H. Mitchell, J. Catal. 78 (1982) 116.
[12] T.M. Duncan, P. Winslow and A.T. Bell, J. Catal. 43 (1985) 1.
[13] D.W. Goodman and J.T. Yates, Jr., J. Catal. 82 (1983) 225.
[14] M. Logan, A.J. Gellman and G.A. Somorjai, J. Catal. 94 (1985) 60.
[15] J.L. Hérisson and Y. Chauvin, Makromol. Chem. 141 (1970) 161.
[16] J.P. Soufflet, D. Commercue and Y. Chauvin, C.R. Hebd. Séances Acad. Sci., Ser. C. 276 (1973) 169.
[17] R.J. Haines and G.J. Leigh, Chem. Soc. Rev. 4 (1975) 155.
[18] C.P. Casey and J. Burkhardt, J. Am. Chem. Soc. 96 (1974) 7808.
[19] E.O. Fischer and K.H. Dotz, Chem. Ber. 105 (1972) 3966.
[20] R.R. Schrock, J. Am. Chem. Soc. 96 (1974) 6976.
[21] R.R. Schrock, J. Am. Chem. Soc. 98 (1976) 5399.
[22] B.A. Dolgoplosk, Dokl. Chem. 216 (1974) 380.
[23] R.H. Grubbs, P.L. Burk and D.D. Carr, J. Am. Chem. Soc. 97 (1975) 3265.
[24] R.H. Grubbs, D.D. Carr, C. Hoppin and P.C. Burk, J. Am. Chem. Soc. 98 (1976) 3478.
[25] T.J. Katz and J. Rothschild, J. Am. Chem. Soc. 98 (1976) 2519.
[26] T.J. Katz and W.H. Hersch, Tet. Lett. (1977) 585.
[27] C.P. Casey, H.E. Tuinstra and M.C. Saeman, J. Am. Chem. Soc. 98 (1976) 608.
[28] F.N. Tebbe, G.W. Parshall and D.W. Ovenall, J. Am. Chem. Soc. 101 (1979) 5074.
[29] J. Wengorius, R.R. Schrock, M.R. Churchill, J.R. Mussert and W.J. Young, J. Am. Chem. Soc. 102 (1980) 4515.
[30] T.R. Howard, J.B. Lee and R.H. Grubbs, J. Am. Chem. Soc. 102 (1980) 6878.
[31] R.H. Grubbs and T.K. Brunck, J. Am. Chem. Soc. 94 (1972) 25.
[32] B. Bartlett, V.L. Schneerson and W.T. Tysoe, Catal. Lett. 3 (1995) 1.
[33] B.F. Bartlett, C. Soto, H. Molero and W.T. Tysoe, J. Catal., submitted for publication.
[34] J.B. Claridge, M.L. Green, S.C. Tsang and A.P.E. York, Appl. Catal. 89 (1992) 103.
[35] L. Wang, L. Tao, M. Xie and Y. Xu, Catal. Lett. 21 (1993) 35.
[36] F. Solymosi, E. Erdohelyi and A. Szoke, Catal. Lett. 32 (1995) 43.
[37] R.L. Burwell and A.J. Brenner, J. Mol. Catal. 1 (1975) 77.
[38] R. Thomas and J.A. Moulŷn, J. Mol. Catal. 15 (1982) 157.
[39] W.T. Tysoe, Langmuir 12 (1996) 78.
[40] F. Zaera, Acc. Chem. Res. 25 (1992) 260.
[41] F. Zaera, J. Mol. Catal. 86 (1994) 221.
[42] F. Zaera, Chem. Rev. 95 (1995) 2651.
[43] X.-L. Zhou, X.-Y. Zhu and J.M. White, Acc. Chem. Res. 23 (1990) 237.

[44] M.K. Weldon and C.M. Friend, Surf. Sci. 321 (1994) L202.
[45] H.M. Kennett and A.E. Lee, Surf. Sci. 48 (1975) 591.
[46] H.M. Kennett and A.E. Lee, Surf. Sci. 48 (1975) 606.
[47] H.M. Kennett and A.E. Lee, Surf. Sci. 48 (1975) 617.
[48] H.M. Kennett and A.E. Lee, Surf. Sci. 48 (1975) 624.
[49] H.M. Kennett and A.E. Lee, Surf. Sci. 48 (1975) 633.
[50] A.E. Lee, Surf. Sci. 47 (1975) 191.
[51] C. Zhang, M.A. Van Hove and G.A. Somorjai, Surf. Sci. 149 (1985) 326.
[52] E. Bauer and H. Poppa, Surf. Sci. 88 (1979) 31.
[53] G. Bredael, F. Zaera and W.T. Tysoe, Langmuir 5 (1989) 899.
[54] L.P. Wang, R. Hinkelman and W.T. Tysoe, J. Electron Spectrosc. Relat. Phenom. 56 (1991) 341.
[55] A.W. Potts, H.J. Lempka, D.G. Streets and W.G. Proce, Philos. Trans. R. Soc. London, A268 (1970) 59.
[56] E.I. Ko and R.J. Madix, Surf. Sci. 109 (1981) 221.
[57] J.-L. Lin, C.-M. Chang, C.J. Jenks, M.X. Yang, T.H. Wentzlaff and B.E. Bent, J. Catal. 147 (1994) 250.
[58] P.M. Loggenberg, L. Carlton, R.G. Copperthwaite and G.J. Hutchins, J. Chem. Soc., Chem. Commun. (1987) 541.
[59] X.-L. Zhou and J.M. White, J. Phys. Chem. 95 (1991) 5575.
[60] C.J. Jenks, J. Lin, C. Chiang, L. Kang, P.S. Laeng, T.H. Wentzlaff and B.E. Bent, Structure-Activity and Selectivity in Heterogeneous Catalysis, Eds. R.K. Graselli and A.W. Sleight (Elsevier, Amsterdam, 1991).
[61] C.-M. Chang, T.H. Wentslaff and B.E. Bent, J. Phys. Chem. 96 (1992) 1836.
[62] C. Zheng, Y. Apeloig and R. Hoffmann, J. Am. Chem. Soc. 110 (1988) 749.
[63] F.A. Cotton and G. Wilkinson, Advanced Inorganic Chemistry (Interscience, London, 1968).
[64] P.A. Redhead, Vacuum 12 (1962) 203.
[65] H.R. Han and L.D. Schmidt, J. Phys. Chem. 75 (1971) 227.
[66] Weast, R.C. (Ed.) Handbook of Chemistry and Physics (Chemical Rubber Co., Cleveland, 1967).
[67] J.L. Grant, T.B. Fryberger and P.C. Stair, Surf. Sci. 159 (1985) 333.